Attenuated Total Reflectance Fourier Transform Infrared Studies of the Interaction of Melittin, Two Fragments of Melittin, and δ-Hemolysin with Phosphatidylcholines†

Joseph W. Brauner,‡ Richard Mendelsohn,*,‡ and Franklyn G. Prendergast*,§

Department of Chemistry, Rutgers University, Newark, New Jersey 07102, and Department of Biochemistry and Molecular Biology, Mayo Medical School, Rochester, Minnesota 55905

Received May 21, 1987; Revised Manuscript Received August 11, 1987

ABSTRACT: Attenuated total reflectance Fourier transform infrared spectroscopy (ATR FT-IR) has been used to monitor alterations in phospholipid organization in thin layers of 1,2-dipalmitoylphosphatidylcholine (DPPC) and 1-palmitoyl-2-oleoylphosphatidylcholine (POPC), induced by the membrane lytic peptide melittin, its fragments 1–15 (hydrophobic fragment) and 16–26 (hydrophilic fragment), and δ-hemolysin. In addition, the secondary structures of the peptides and the orientation of helical fragments were determined with respect to the bilayer. The insertion of melittin into POPC caused large perturbations in the order and increased rates of motion of the acyl chains, as monitored by the frequency and half-width of the symmetric CH_2 stretching vibration near 2850 cm^{-1}, as well as by the ATR dichroic ratio for this mode. Changes in DPPC organization were less and were consistent with peptide-induced static disordering (gauche rotamer formation) in the acyl chains. Melittin adopted primarily an α-helical secondary structure, although varying small proportions of β and/or aggregated forms were noted. The helical segments were preferentially oriented perpendicular to the bilayer plane. Several modes of melittin/lipid interaction were considered in an attempt to semiquantitatively understand the observed dichroic ratios. By considering the peptide as a bent rigid rod, a plausible model for its lytic properties has been developed. The hydrophilic fragment in DPPC showed a secondary structure with little α-helix present. As judged by its effect on phospholipid acyl chain organizational parameters, the fragment did not penetrate the bilayer substantially. The hydrophobic fragment in DPPC gave amide I spectral patterns consistent with a mixture of predominantly β-antiparallel pleated sheet with a smaller fraction of α-helix. Disordering of the lipid acyl chains was induced by this fragment. δ-Hemolysin exhibited predominantly α-helical secondary structure, with only moderate orientational preference. It is suggested to lie randomly within the bilayer.

Melittin, an amphiphilic 26-amino acid peptide isolated from bee venom, has been widely investigated as a model compound for studies of peptide/lipid and protein/lipid interaction. The peptide induces a wide variety of effects in lipidic environments including increase in ionic permeability, lysis of natural and artificial membranes (Olson et al., 1974; Weissmann et al., 1969), and potentiation of phospholipase A2 activity (Mollay et al., 1976; Yunes et al., 1977).

The structure of melittin in several environments, including the crystalline form, aqueous solution, and reconstituted into micelles or lipid vesicles, has been probed with a plethora of physical methods including X-ray diffraction (Terwilliger et al., 1982), NMR[1] spectroscopy (Dufourc et al., 1976; Lauterwein et al., 1980; Brown et al., 1982), circular dichroism (Bello et al., 1982), fluorescence spectroscopy (Hermetter & Lakowicz, 1986; Vogel & Jahnig, 1986), and vibrational (IR and Raman) spectroscopies (Levin et al., 1982; Verma et al., 1974; Bernard et al., 1982; Dasseux et al., 1984; Lavialle et al., 1982; Vogel et al., 1983; Vogel & Jahnig, 1986). Such studies have shown that melittin can exist in either monomeric or tetrameric forms and that each form may interact with lipid bilayers. Yet many issues are unresolved. The state of association of the peptide in the lipid layer (an important parameter for understanding the lytic mechanism) is still uncertain [for two recent diametrically opposed views, see Hermetter and Lakowicz (1986) and Vogel and Jahnig (1986)]. In addition, no complete picture of the effect of melittin on the ordering and dynamics of phospholipid molecules has been obtained, although the recent NMR experiments of Dufourc et al. (1986) have addressed the latter on the microsecond time scale.

Vibrational spectroscopic techniques have proven to be powerful approaches for probing lipid organization and phase behavior as well as protein/peptide secondary structure in reconstituted model membrane systems (Levin, 1984; Mendelsohn & Mantsch, 1986). Several IR and Raman studies of melittin/lipid interaction have already appeared. The initial IR report by Verma et al. (1974) revealed no linear dichroism of the amide I or II bands in oriented phosphatidylcholine films. In contrast, a reinvestigation of this problem (Vogel

† R.M. acknowledges receipt of Grant GM-29864 from the USPHS in support of this study, while F.G.P. acknowledges receipt of Grant GM-34847 from the same source. Further funds were awarded to R.M. from the Busch bequest of Rutgers University.

* Address correspondence to this author.
‡ Rutgers University.
§ Mayo Medical School.

[1] Abbreviations: ATR, attenuated total reflectance; FT-IR, Fourier transform infrared; DPPC, 1,2-dipalmitoylphosphatidylcholine; POPC, 1-palmitoyl-2-oleoylphosphatidylcholine; MLT_{1-15}, melittin hydrophobic fragment (residues 1–15); MLT_{16-26}, melittin hydrophilic fragment (residues 16–26); $\nu^{sym}_{CH_2}$, frequency of the symmetric CH_2 stretching mode; $\nu^{asym}_{CH_2}$, frequency of the asymmetric CH_2 stretching mode; $\Delta\nu^{sym}_{CH_2}$, half-width of the symmetric CH_2 stretching mode (measured as the full width at half-height); R^{ATR}, ATR dichroic ratio; NMR, nuclear magnetic resonance; HPLC, high-performance liquid chromatography.

0006-2960/87/0426-8151$01.50/0

et al., 1983) suggested the spatial orientation of melittin to be preferentially parallel to the membrane normal. Lavialle et al. (1982) have carried out Raman studies of the amide I spectral region for melittin and melittin-derived peptides 1–19 and 21–26. Finally, Raman spectral data have been used (Vogel & Jahnig, 1986) to semiquantitatively estimate the fraction of α-helix present.

In this study, the powerful techniques of attenuated total reflectance (ATR) coupled with Fourier transform infrared spectroscopy (FT-IR) are used to determine the secondary structure and orientation of melittin and hydrophobic and hydrophilic peptides derived from melittin in oriented phospholipid environments and to determine peptide-induced alterations in lipid structure and orientational order. In addition, the orientation of δ-hemolysin, a membrane lytic peptide from *Staphylococcus aureus*, has been determined.

Experimental Procedures

Materials

DPPC and POPC were purchased from Avanti Polar Lipids, Inc., Birmingham, AL. Samples of DPPC examined by differential scanning calorimetry showed thermotropic behavior in good accord with published data. Melittin (MLT) and two peptide fragments of melittin with sequences H_2N-GIGAVLKVLTTGLPA-OH (MLT_{1-15}) and H_2N-LISWIKRKRQQ-$CONH_2$ (MLT_{16-26}), the hydrophobic and hydrophilic fragments, respectively, were synthesized de novo. For melittin and MLT_{16-26}, *p*-methylbenzhydrylamino–resin was employed as the host resin to afford the carboxy-terminal amide after HF cleavage. All three peptides were synthesized on an Applied Biosystems peptide synthesizer and subsequently purified by HPLC on a C_{18} reverse-phase column with elution with a H_2O/acetonitrile gradient. Purity was determined by use of fast atom bombardment mass spectrometry in the laboratory of Dr. Ian Jardine (Department of Pharmacology, Mayo Foundation). Melittin and the fragments showed no impurities; sequencing on an Applied Biosystem sequence verified the amino acid sequences. The *Staphylococcus aureus* (Foggi stain) δ-hemolysin was a gift from Dr. J. Fitton; this peptide gave a single peak on reverse-phase HPLC, and there were no impurities in the fast atom bombardment mass spectrum.

Methods

Coating of the ATR Crystals. The orientation of lipids and peptides was studied on Ge ATR crystals possessing either hydrophilic or hydrophobic surfaces. The latter were prepared according to Kahn (1973), with the silanizing reagent octadecyldimethyl[3-(trimethoxysilyl)propyl]ammonium chloride, 50% in MeOH, obtained from Petrarch Systems, Inc., Bristol, PA.

ATR Films. Pure lipids were dissolved in $CHCl_3$ at a concentration of 1 mg/mL. Lipid/peptide mixtures were prepared by dissolving them together in a 4:1 $CHCl_3$/MeOH mixture such that the lipid/peptide ratio was about 10:1.

A total of 25 μL of the resulting solution was applied to one face of the Ge ATR crystal. Capillary attraction to a clean Teflon bar was used to move the solution back and forth along the surface until the solvent evaporated. An iridescent film (gold-brown or bluish brown in reflection) was sought. When the original solvent mixture was $CHCl_3$/MeOH, it was necessary to rework the deposited film with pure $CHCl_3$ in order to achieve the desired result. The same procedure was duplicated on the other face of the ATR crystal. Noniridescent films (usually streaky white in appearance) are apparently in poor optical contact with the surface and usually result in poor FT-IR spectral data.

FT-IR. Spectra were obtained on a Mattson Instruments Sirius 100 spectrometer equipped with a Hg–Cd–Te detector. A total of 200 interferograms were collected, coadded, apodized with a triangular function, and fast Fourier transformed to give 4-cm^{-1} resolution. Peak positions were determined with a three-point parabolic peak-picking routine supplied with the instrument software. Polarization data were acquired with a wire grid polarizer.

As the amide I region in these samples consisted of overlapped bands from more than one conformation with differing dichroic ratios, meaningful ATR measurements could only be obtained with band-resolving procedures. Bands were simulated with line-shape functions that were 50:50 Gaussian/Lorentzian mixtures. Positions, bandwidths, and amplitudes were varied until good agreement was achieved between actual and simulated spectra (see Figure 2B). Dichroic ratios were measured as integrated band area ratios. Peak height ratios do not in general agree with ratios obtained from band areas and, hence, cannot be used to determine R^{ATR} unless the band in question is sufficiently isolated. Areas of the component bands were taken over the spectral range where the decomposition was performed.

It was determined that measurements of R^{ATR}_{2850} did not require curve resolving procedures while for R^{ATR}_{2920} this was approximately true. When peak heights were used for the former, a linear base line was drawn between 2830 and 2870 cm^{-1}, and the vertical height was measured from the base line to the peak maximum near 2850 cm^{-1} in the flattened spectrum.

For three cases (DPPC/melittin and DPPC/MLT_{1-15}, Table II) where the C–H spectral region was fit with six bands as suggested by Snyder et al. (1978), R^{ATR}_{2850} exactly agreed with R^{ATR}_{2920}. This exact agreement was anticipated since both bands have transition moments perpendicular to the main acyl chain axis. R^{ATR}_{2920} values for pure lipid samples (Table I) were measured as peak height ratios. While the agreement with R^{ATR}_{2850} was within experimental error, the use of band decomposition procedures produces even better accord.

Results

Oriented Lipid Bilayers. To establish base-line levels for the degree of phospholipid orientational order that could be achieved in peptide-free systems, films of DPPC and POPC were cast on both silanized and unsilanized germanium surfaces. Lipid orientational order was determined from ATR dichroic ratios (R^{ATR}, as defined in the Appendix) of the acyl chain CH_2 symmetric and antisymmetric stretching vibrations, near 2850 and 2920 cm^{-1}, respectively. Our experimental geometry is shown in Figure A1 (Appendix). Typical dichroic spectra for DPPC in the region 2800–3000 cm^{-1} are shown in Figure 1. The origin of the spectral features is well established (Mendelsohn & Mantsch, 1986). The asymmetric and symmetric CH_3 stretching modes appear near 2956 and 2872 cm^{-1}, respectively, while the antisymmetric and symmetric CH_2 stretching bands are observed at 2920 and 2850 cm^{-1} (Cameron et al., 1980), along with a broad Fermi resonance band (Snyder et al., 1978) centered near 2900 cm^{-1}. The frequencies ($\nu^{sym}_{CH_2}$) and half-widths ($\Delta\nu^{sym}_{CH_2}$) for the symmetric stretching mode and R^{ATR}_{2850} and R^{ATR}_{2920} are given for DPPC and POPC in Table I. The frequencies and half-widths of these bands are known to be sensitive to changes in the configuration of the acyl chains. For example, during the gel–liquid crystal phase transition of DPPC, $\nu^{sym}_{CH_2}$ increases by about 4 cm^{-1} and its half-width increases by 3.5 cm^{-1} (Cameron et al., 1980).

Table I: Frequencies, Half-Widths, and ATR Dichroic Ratios for DPPC and POPC[a]

sample	crystal	$\nu^{sym}_{CH_2}$ (cm^{-1})	$\Delta\nu^{sym}_{CH_2}$ (cm^{-1})	R^{ATR}_{2850}	R^{ATR}_{2920}
DPPC	s	2850.4 ± 0.1 (8)	9.9 ± 0.3 (8)	1.00 ± 0.04 (4)	0.99 ± 0.07 (4)
	u	2850.4 ± 0.1 (4)	9.9 ± 0.2 (4)	1.12 ± 0.01 (4)	1.13 ± 0.01 (4)
POPC	s	2851.4 ± 0.1 (4)	11.5 ± 0.04 (4)	1.09 ± 0.05 (4)	1.15 ± 0.03 (4)
	u	2851.1 ± 0.2 (4)	11.0 ± 0.6 (4)	1.12 ± 0.03 (4)	1.18 ± 0.04 (4)

[a] Germanium crystal; s = silanized (hydrophobic surface) and u = unsilanized (hydrophilic) surface. $\nu^{sym}_{CH_2}$ and $\Delta\nu^{sym}_{CH_2}$ stand for the frequency and half-width (full width at half-height) respectively of the CH_2 symmetric stretching mode. Figure in parentheses after each standard deviation = the number of measurements. R^{ATR}_{2850} and R^{ATR}_{2920} stand for the ATR dichroic ratios as discussed in the text for the symmetric and asymmetric CH_2 stretching vibrations, respectively.

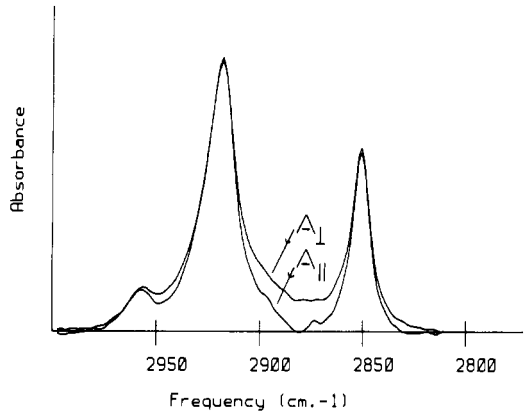

FIGURE 1: Polarized FT-IR ATR data for the CH_2 stretching region of DPPC. The parallel and perpendicular components are indicated on the figure and correspond to our experimental geometry as outlined in the Appendix and shown in Figure A1. Note that the band at 2850 cm^{-1}, the prime indicator of lipid order, is well isolated from other spectral features. Hence, curve decomposition procedures are not required for estimation of its intensity.

Instrumental precision for the current measurements of frequency is estimated to be better than 0.02 cm^{-1}. Standard deviations (Table I) for four or eight measurements of $\nu^{sym}_{CH_2}$ indicate that experimental reproducibility is high, this parameter being determined with a precision of about 0.1 cm^{-1} for DPPC and about 0.2 cm^{-1} for POPC. The reproducibility in the half-width measurement is somewhat worse, a result of sample-to-sample variation in the establishment of consistent spectral base lines. Thus, although changes in lipid physical state produce only relatively small frequency and half-width increases, these parameters are useful as indicators of structural reorganizations in the lipid phase as a consequence of melittin insertion as they can be monitored with a precision 10–20 times the change observed.

The transition moments for both $\nu^{sym}_{CH_2}$ and $\nu^{asym}_{CH_2}$ lie at right angles to the acyl chain axis (Fringeli & Gunthard, 1981). As the introduction of disorder (through the formation of gauche rotamers) into the acyl chains alters the direction of the main chain with respect to the ATR crystal z axis (Figure A1), the dichroic ratio is expected to provide a third sensitive indicator of acyl chain order. The order parameter derived from the measured dichroic ratio expected for this direction transition moment is given by the $\alpha = 90°$ curve in Figure A2 (Appendix). The results in Table I show that the most highly ordered ATR samples are DPPC on silanized Ge. The average acyl chain angle of disorientation is estimated from eq A3 applied to the 2850-cm^{-1} band (Table I) to be 28° (with error limits of +9 or −7 deg). These results are in good accord with X-ray diffraction studies of Janiak et al. (1976) and in excellent agreement with a previous IR investigation of oriented lipid films (Okamura et al., 1986).

In contrast to the high degree of orientational order observed for DPPC (expected because the molecule has its acyl chains in the all-trans configuration under the experimental conditions), POPC films on both unsilanized and silanized Ge demonstrate an average angle of disorientation (46–55°, see Table I and the Appendix) close to that expected for a random distribution of CH_2 groups with respect to the bilayer normal. The latter will produce an angle of 54.7°. This result is reasonable as POPC is well above its T_m (2 °C for a fully hydrated sample) under the conditions of the experiment and thus contains substantial numbers of gauche rotamers which (on average) reorient the acyl chains away from the z direction. Further evidence for acyl chain disorder in POPC comes from the rather high symmetric stretching frequencies, dichroic ratios, and half-widths compared with those of DPPC, as expected (Mendelsohn & Mantsch, 1986) for a molecule in the liquid crystalline state.

Table II: ATR Parameters for Lipid/Peptide Complexes[a]

sample	crystal	$\nu^{sym}_{CH_2}$ (cm^{-1})	$\Delta\nu^{sym}_{CH_2}$ (cm^{-1})	R^{ATR}_{2850}	R^{ATR}_{2920}
DPPC/melittin	s	2850.8	9.7	1.33	1.34
DPPC/melittin	u	2850.7	9.9	1.25	1.24
DPPC/MLT_{16-26}	s	2850.7	9.7	1.07	
DPPC/MLT_{1-15}	u	2850.8	11.5	1.19	1.19
POPC/melittin	s	2853.9	13.2	1.50	
DPPC/δ-hemolysin	s	2850.9	9.7	1.15	

[a] Germanium crystal; s = silanized (hydrophobic) surface and u = unsilanized (hydrophilic) surface. Spectral parameters are as defined in Table I.

Effect of Melittin and Its Fragments on Phosphatidylcholine Acyl Chain Ordering. The effects of melittin and its fragments on acyl chain order in DPPC and POPC are summarized in Table II. Insertion of melittin or its hydrophobic fragment 1–15 into DPPC produces substantial increases for R^{ATR}_{2850} and R^{ATR}_{2920}, the effect being greater for the complete peptide. In contrast, the hydrophilic fragment 16–26 induces little or no alteration in this parameter. Melittin and its fragments all induce a slight increase in $\nu^{sym}_{CH_2}$, whereas only the hydrophobic fragment causes a significant increase in $\Delta\nu^{sym}_{CH_2}$.

The effects on acyl chain order induced by melittin in films of POPC are substantially different from those observed in DPPC samples. Relatively large increases are noted in $\nu^{sym}_{CH_2}$, $\Delta\nu^{sym}_{CH_2}$, and R^{ATR}_{2850}. These observations are discussed below. It is noted that an earlier IR linear dichroism study (Vogel & Jahnig, 1983) could not determine changes in lipid spectral parameters upon melittin insertion. The additional precision inherent in the FT-IR experiment is evident in the current work.

Melittin Secondary Structure and Orientation in Lipid Environments. ATR dichroic spectra for films of a DPPC/melittin complex are shown in Figure 2A. The spectral region plotted, 1800–1400 cm^{-1}, contains the lipid carbonyl C=O stretching mode (1710–1750 cm^{-1}), the peptide bond amide I mode (1620–1680 cm^{-1}, mostly a peptide bond C=O stretching vibration), the peptide bond amide II mode (1520–1560 cm^{-1}, mostly a mixture of peptide bond C–N stretch and N–H in-plane bend), and the lipid acyl chain CH_2

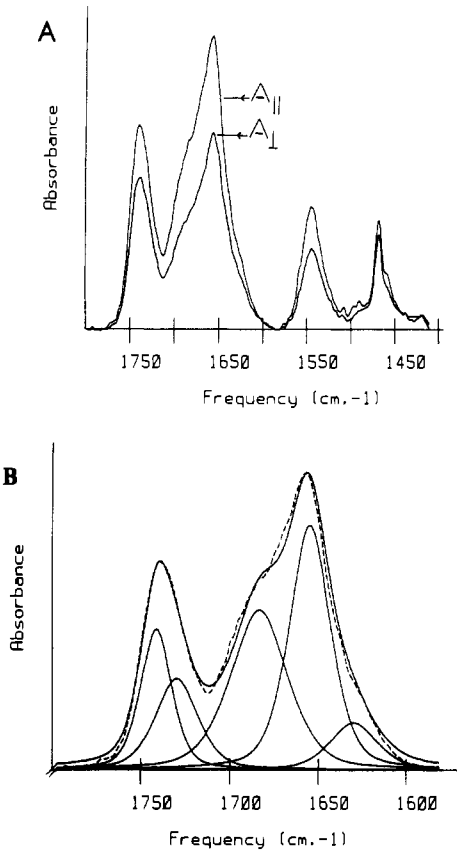

FIGURE 2: (A) Polarized FT-IR ATR data for melittin in DPPC, showing a pair of bands (shoulders) near 1680 and 1630 cm^{-1}, characteristic of β-type secondary structure, and a main α-helical feature near 1656 cm^{-1}. Measurement of the dichroic ratio for the α-helical feature required curve decomposition protocols, as the β-type bands were strongly overlapped with the 1656-cm^{-1} feature and showed different dichroic ratios. (B) Demonstration of the band decomposition procedure for the parallel component of a DPPC/melittin sample. The dashed line is the observed spectrum. The five component bands (solid lines) have been added together to produce a resultant spectrum (also indicated by a solid line) that matches the observed spectrum quite closely.

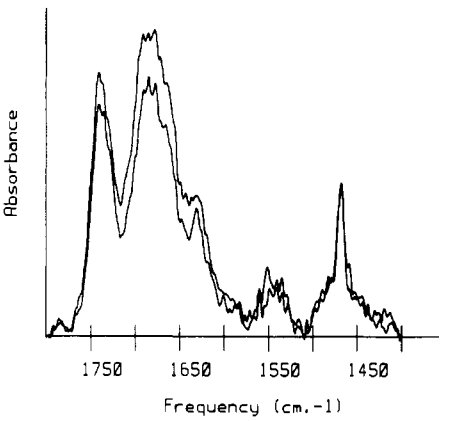

FIGURE 3: Polarized FT-IR ATR data for the hydrophilic fragment of melittin in DPPC. Little intensity characteristic of an α-helix is evident at 1656 cm^{-1}. The observed features are tentatively suggest to arise from an aggregated form on the lipid surface. The more intense spectrum is the parallel component; the weaker spectrum is the perpendicular component.

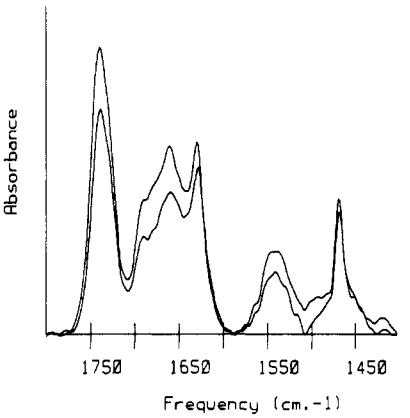

FIGURE 4: Polarized FT-IR ATR data for the hydrophobic fragment of melittin in DPPC. The intense feature at 1630 cm^{-1}, along with the weaker band at 1680 cm^{-1}, taken as a pair, indicates that the dominant secondary structure is β-antiparallel pleated sheet. A significant contribution at 1660 cm^{-1} is due to α-helix. The more intense spectrum is the parallel component; the weaker spectrum is the perpendicular component.

bending mode (1450–1480 cm^{-1}). Typical results for our band decomposition protocol using a 50:50 Gaussian/Lorentzian function to simulate the band shapes for the 1800–1600-cm^{-1} region are shown in Figure 2B. The R_{1656}^{ATR} values for the component of the amide I vibration near 1656 cm^{-1} were as follows: melittin/DPPC, 1.46 ± 0.03 (six measurements); melittin/POPC, 1.20 (three measurements); melittin (lipid-free film), 1.17 (three measurements); δ-hemolysin/DPPC, 1.34 ± 0.06 (six measurements).

For lipid-free films of pure melittin (data not shown), the amide I contour consisted of a strong feature with a peak at 1656 cm^{-1}. Minor contributions at 1630 and 1685 cm^{-1} can be discerned with curve resolving procedures. The major amide I component (1656 cm^{-1}) indicates that either a random coil or an α-helical secondary structure predominates. The uncertainty arises as the amide I frequencies for these secondary structures are quite similar in the IR. If the helical structure is indeed present, the measured dichroic ratio of 1.17 indicates random orientation of the peptide bonds with respect to the normal to the Ge crystal face. If the random coil structure is present, a random orientation of transition moments will result in a dichroic ratio close to 1.18, regardless of any preferential molecular orientation. Spectra of small (15 μm) melittin crystals taken with an FT-IR microscope (R. Mendelsohn and J. Brauner, unpublished results) show an amide I pattern very similar to that of the ATR film. As the crystals are known (Terwilliger et al., 1982) to have a large fraction of α-helical secondary structure, that conformation is suggested for the film.

Melittin/phospholipid complexes show amide I contours altered from those of pure melittin. Some samples (such as shown in Figure 2A), showed clear shoulders at 1680 and 1630 cm^{-1} in addition to the main feature at 1656 cm^{-1}. Other samples (data not presented) showed primarily the latter band, although there were vestiges evident of the low- and high-frequency shoulders. Unlike R_{1656}^{ATR} for the pure melittin film, R_{1656}^{ATR} for melittin/DPPC is indicative of substantial orientation of the α-helical secondary structure perpendicular to the bilayer plane. Quantitative aspects are discussed below. The structural origin of the features near 1630 and 1680 cm^{-1} is unclear. Although the frequencies might be appropriate for a β-antiparallel pleated sheet, the relative intensities are reversed from those normally found for that secondary structure.

Secondary Structure of Melittin Fragments 1–15 and 16–26. Spectra of the amide I region for the two melittin fragments in DPPC are shown in Figures 3 and 4. Similar data (not shown) were obtained for these molecules in POPC. The hydrophilic fragment (Figure 3) showed an intense band near 1685 cm^{-1}, a weaker feature near 1630 cm^{-1}, and only little intensity at the helical frequency of 1656 cm^{-1}. The observed amide I contour is consistent with little random coil

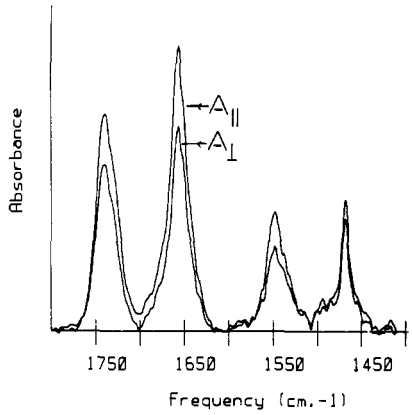

FIGURE 5: Polarized FT-IR ATR data for δ-hemolysin in DPPC. The α-helical band at 1657 cm^{-1} is very intense and sharp, indicative of a homogeneous environment.

or α-helix present in the secondary structure. The origin of the strong feature at 1685 cm^{-1} is unknown. It is speculated that it arises from molecules aggregated at the lipid surface in an extended type of conformation.

The hydrophobic fragment (Figure 4) shows a complex amide I pattern, the main contributors to which are bands arising from β-antiparallel pleated sheet (1685 and 1630 cm^{-1} in the correct intensity ratio for this secondary structure) and α-helix (1660 cm^{-1}).

δ-Hemolysin. Films of δ-hemolysin incorporated into DPPC at a lipid/protein mole ratio of 10:1 exhibited a high degree of bluish brown iridescence, a criterion reported (Fringeli & Gunthard, 1981) to be indicative of a high degree of homogeneity. Spectra of the 1400–1800-cm^{-1} region are shown in Figure 5. The observed intense, sharp band at 1657 cm^{-1} is appropriate for either an α-helix or a random coil secondary structure. The observed sharpness of the feature and nonrandom polarization induce us to strongly prefer the former assignment. Curve resolving procedures show minor contributions at 1635 and 1680 cm^{-1}. The low intensity of these components indicates that the peptide largely adopts the α-helical conformation. The weak bands at 1635 and 1680 cm^{-1}, taken as a pair, are indicative of a small fraction of β-antiparallel pleated sheet secondary structure. The measured value of R_{1657}^{ATR} is 1.34 ± 0.06 (average of six independent measurements).

Discussion

NMR studies of Dufourc et al. (1986) have revealed substantial differences in the ability of melittin to interact with gel-phase or fluid-phase lipids. In the current investigation, the perturbations induced by melittin on lipid structure are much stronger for POPC than for DPPC. All POPC lipid parameters ($\nu_{CH_2}^{sym}$, $\Delta\nu_{CH_2}^{asym}$, and R_{2850}^{ATR}) are substantially altered by melittin incorporation. The spectral changes are internally consistent in that each reveals a substantial peptide-induced disordering (increase in the number of gauche rotamers) of the lipid acyl chains. The high value of R_{2850}^{ATR}, 1.50 (which lies slightly above the maximum for the $\alpha = 90°$ curve in Figure A2), implies preferential orientation of the POPC acyl chains parallel to the original bilayer plane. This in turn suggests that melittin completely disrupts the bilayer. Dufourc et al. (1986) suggest that at $T > T_m$ an apparent general chain disordering is noted at lipid/protein ratios of >20. In addition, they conclude that at lipid/protein ratios of 4 large lamellar lipid phases do not exist; formation of small structures is suggested. In the current work, the lack of full hydration and the presence of a hydrophobic surface probably preclude formation of such structures but may simply lead to substantial disruption of the lipid bilayer. The melittin itself is primarily in the α-helical conformation, but little or no preferential orientation of the helical axis ($R_{1656}^{ATR} = 1.20$, compared with 1.17 for randomly oriented molecules as observed in pure melittin films) is noted, consistent with a disrupted bilayer structure.

The effects of melittin on lipid order in DPPC/melittin complexes are in sharp contrast to those for POPC. Little change is observed in $\Delta\nu_{CH_2}^{sym}$, while $\nu_{CH_2}^{sym}$ increases only slightly. However, a substantial increase in R_{2850}^{ATR} from 1.00 and 1.33 (suggestive of acyl chain preferential orientation more parallel to the bilayer plane than in the protein-free system) is noted. In addition, the helical segments of melittin are quite highly oriented perpendicular to the bilayer plane, as indicated by R_{1656}^{ATR} of 1.46.

To explain the change in the lipid parameters, we note that increases in $\nu_{CH_2}^{sym}$ for lipid bilayers are typically very slight until a relatively large fraction of the lipid has melted. This phenomenon has been modeled elsewhere (Dluhy et al., 1983). That is, the frequency increase in $\nu_{CH_2}^{sym}$ observed when gauche rotamers are introduced is a highly nonlinear function of the number of gauche rotations. In contrast, the band half-width, thought to be sensitive primarily to rates of molecular motion rather than to the formation of gauche rotamers (Mendelsohn et al., 1981), is a more linear function of fractional melting. Thus, the data for DPPC/melittin complexes suggest the following: The slight increase in $\nu_{CH_2}^{sym}$ indicates that gauche rotations are induced in the acyl chains. This disordering, while sufficient to drastically alter the average chain direction as measured by R_{2850}^{ATR}, is not accompanied by an increase in the rate of acyl chain motion, as shown by the constancy or slight decrease of the half-widths. Thus, the disordering is static in nature. In contrast, the data for POPC suggest a rather large increase in motional rates upon peptide insertion.

Although absolute determination of peptide orientation cannot be accomplished from the single measured ATR parameter, R_{1656}^{ATR} can be compared with that predicted for several possible structural models of melittin orientation in DPPC. First, models with the helical component of melittin oriented parallel to the bilayer plane (Terwilliger et al., 1982) are fairly rigorously excluded by the current measurements. For such cases, R_{1656}^{ATR} [independent of whether the chosen value of the transition moment angle with respect to the helix axis is 22° (Nabedryk et al., 1982), 27.6° (Suzuki, 1971), or 37° (Tsuboi, 1962)] would be substantially less than about 1.10, inconsistent with the current data. Similar conclusions have been reached by Vogel et al. (1983).

It is more difficult to distinguish between models that propose insertion of melittin into the lipid bilayers. The structure of the peptide (Terwilliger et al., 1982) suggests that in crystalline melittin residues 1–10 and 14–26 form two α-helices, with an angle of 120° between their axes. NMR studies of detergent-bound melittin (Brown et al., 1982) suggest that residues 21–26 adopt no well-ordered secondary structure. Thus, residues 1–21 are suggested to retain their helical structure with a hinge between residues 11–13. If the latter model is accepted, then the five peptide bonds connecting residues 21–26 are assumed to have random orientations with respect to the bilayer plane. Several assumptions are now possible. Following Vogel et al. (1983), we may now further assume that the two melittin helices traverse the bilayer, each helix making on average the same angle with the normal to the bilayer. Under these conditions, the value of R_{1656}^{ATR} calculated for the helical segments only (appropriately weighted

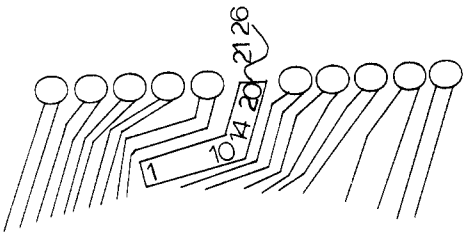

FIGURE 6: A highly schematic depiction of the rigid bent rod model for melittin in DPPC. The numbers are those in the amino acid sequence of melittin.

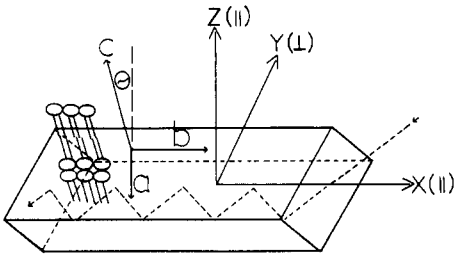

FIGURE A1: Geometric setup and definition of the axis systems used in the current investigation. The crystal used in the current work is germanium.

and calculated from the experimental value of 1.46, assuming that residues 21–26 have $R = 1.18$) is 1.65, so that each will assume an angle of about 35° with the normal to the bilayer. This in turn suggests an angle of 110° between peptide segments, in reasonable accord with the X-ray determination of 120°.

A more realistic model envisions the two helical segments as forming a rigid bent rod with one of the segments (residues 14–20) anchored to the bilayer by the hydrophilic residues 21–26. The angle between segments 1–11 and 14–21 is taken to be 120°. The intensity/peptide bond is assumed to be independent of secondary structure so that

$$R_{EXPTL} = 1.46 = \frac{N_1R_1 + N_2R_2 + N_3R_3}{N_1 + N_2 + N_3}$$

R_1 is the dichroic ratio for the five peptide bonds ($N_1 = 5$) between residues 21 and 26, which equals 1.18 as obtained by setting $f = 0$ in eq A3. R_2 is the dichroic ratio of the seven peptide bonds ($N_2 = 7$) between residues 14 and 21, which form a helix whose axis is assumed to be tilted with an average angle $\bar{\theta}$ to the bilayer normal. R_2 is calculated from eq A3 for an assumed angle α between the helix axis and the transition moment and for a given $\bar{\theta}$. R_3 is the dichroic ratio of the 10 peptide bonds ($N_3 = 10$) between residues 1 and 11 and is calculated from eq A4, where α is the angle between the transition moment and the z' axis. The θ_c used to compute f in eq A4 is fixed (at 60°) by the 120° bend between the top and bottom helices, and θ is taken to be the same as the $\bar{\theta}$ used in computing f in R_2.

The model was used to find the value of θ that gives the experimentally observed dichroic ratio of 1.46 for the 1656-cm^{-1} band of melittin in DPPC. Two values of α, 22° (Nabedryk et al., 1982) and 37° (Tsuboi et al., 1962), were used. No value of θ could reproduce $R_{1656}^{ATR} = 1.46$ when α was set to 37°. For $\alpha = 22°$ the value of θ that reproduced R_{1656}^{ATR} was about 18°. This value is close to that observed for the acyl chain tilt angle from the bilayer normal for phospholipids in standard gel-phase bilayers. With the attached helical segment (1–11) of the melittin making an angle of 60° with this axis, the potential for bilayer disruption is substantial, especially if rotation of this segment occurs about the tilted axis. As these suggestions are consistent with the large perturbation induced in acyl chain orientational order by melittin (Tables I and II), it is not unreasonable to suggest that the rigid bent rod model may begin to account for the membrane lytic properties of the peptide. A highly schematic depiction of these suggestions is shown in Figure 6.

The hydrophilic molecule produces very little perturbation of the lipid spectral parameters and so must be assumed to lie aggregated on the polar lipid surface. The hydrophobic fragment produces about the same change as melittin in $\nu_{CH_2}^{sym}$, but a greater change in $\Delta\nu_{CH_2}^{sym}$ and a smaller change in the dichroic ratios. Some penetration of the molecule into the bilayer is indicated and presumably arises from the α-helical population. However, the majority of the peptide exists in the β-antiparallel pleated sheet structure, which is speculated to lie on the lipid surface. The origin of the increased half-width for this fragment compared with that of intact melittin is unclear.

Thus although intact melittin (in largely α-helical form) can penetrate the lipid bilayer very efficiently and disrupt the orientation of the acyl chains, the hydrophobic peptide MLT_{1-15} (which has a much higher proportion of β-structure and is assumed to lie on the bilayer surface) does not alter the orientation as markedly. The ability of melittin to insert into DPPC under the current experimental conditions is evidently enhanced by the presence of the hydrophilic moiety. Similar observations have been made by Gremlich et al. (1984) in studies of peptides derived from the adrenocorticotropic hormone. The role of hydration in controlling this phenomenon must be explored. Evidence for an active role of water comes from a comparison of the current work with the study of Lavialle et al. (1982), who noted that melittin fragment 1–19 adopts primarily a helical conformation in phospholipid preparations containing excess water. In the current study, we have noted some sample-to-sample variation in the melittin secondary structure in melittin/DPPC complexes. This may be attributable to the solvent (and solvent water content) from which the film was cast. Some samples (such as shown in Figure 2A) contain substantial fractions of nonhelical secondary structures as shown by fairly intense shoulders near 1630 and 1680 cm^{-1}. These are attributed to a fractional population of peptide molecules that lie on the lipid surface in some type of aggregated form, unable to penetrate into the hydrophobic regions of the lipid. Such shoulders are evident in spectra published by other groups but were not commented upon; see, for example, Figure 1 of Vogel et al. (1983). Other samples (data not shown) show much weaker shoulders.

The effect of δ-hemolysin on the DPPC spectral parameters is somewhat less than that induced by melittin. R_{2850}^{ATR} is less changed, while $\nu_{CH_2}^{sym}$ and $\Delta\nu_{CH_2}^{sym}$ are affected similarly. The α-helix of δ-hemolysin is not strongly preferentially oriented perpendicular to the bilayer plane. The observed R_{1656}^{ATR} of 1.34 leads to an average angle of disorientation of about 47° (not far from the random "magic" angle of 54.7°), suggestive of a less uniform state than that adopted by melittin. It is speculated that δ-hemolysin penetrates the bilayer and is randomly distributed within.

It is not possible with the current measurements to obtain independent information on the orientation of the two helical segments of melittin, and hence to test the details of the models proposed for peptide insertion. Current work involves synthesis of melittin derivatives with ^{13}C inserted at particular peptide bond carbons. The peptide bond amide I frequency will, with ^{13}C present, shift into a relatively free spectral region (about 1610 cm^{-1}), and orientations at particular peptide sites will become precisely determined. Finally, the utility of high-

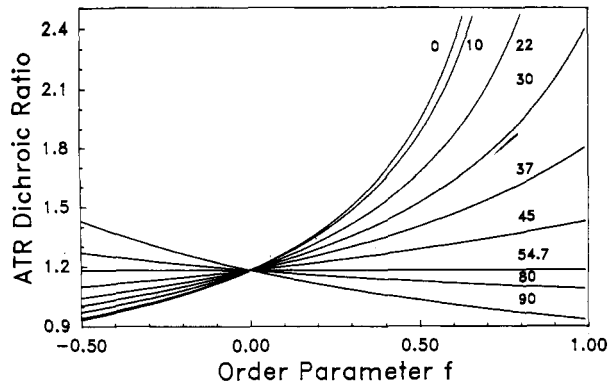

FIGURE A2: Our parametric plot of R^{ATR} as a function of f [recall that $f = (3\cos^2\theta - 1)/2$] for various values of α, the transition moment direction with respect to the helix axis. Further details are given in the Appendix.

precision ATR FT-IR data for following mutually induced alterations in lipid and peptide organization and structure augurs well for further applications of this method.

ACKNOWLEDGMENTS

Dr. John Fitton of ICI (U.K.) graciously supplied a sample of δ-hemolysin.

APPENDIX

Infrared Dichroism in Uniaxially Oriented Thin Films. As the various groups utilizing ATR IR spectroscopy apply different methods to analyze dichroism data, it seemed appropriate for us to describe our procedures in reasonable detail. A thin film is spread on an IR transmitting crystal such as Ge with the beam passing through the crystal via multiple internal reflections, as depicted in Figure A1. An exponentially decaying evanescent wave emerges for a distance the order of a wavelength at each reflection and so can be absorbed by material on the crystal surface. This attenuated total reflection can be studied with polarized light. The ATR dichroic ratio R^{ATR} is defined for a particular absorption band as the ratio of the integrated intensity of the radiation polarized parallel to plane of incidence to that polarized perpendicular. For the coordinate system shown in Figure A1

$$R^{ATR} = \frac{A_\parallel}{A_\perp} = \frac{E_x^2 k_x + E_z^2 k_z}{E_y^2 k_y} \tag{A1}$$

where E_x is the the electric field amplitude in the x direction and k_x is the integrated absorption coefficient in the x direction, with similar quantities defined for y and z.

Following Fraser (1953), we attach a set of axes a, b, and c to the molecules such that the c axis coincides with the chain (rod axis) direction and a and b are perpendicular to the chain and to each other. The direction of the c axis is related to the z axis by a polar angle θ_c and an azimuthal angle ϕ_c, and similarly for the a and b axes.

We assume fiber-type orientation, that is, all ϕ values equally probable. The z axis is the fiber axis for this uniaxial distribution. We assume that all directions about the c axis are equally probable. For this case

$$\begin{aligned} k_z &= KM^2[f\cos^2\alpha + (1/3)(1-f)] \\ k_x = k_y &= KM^2[(1/2)f\sin^2\alpha + (1/3)(1-f)] \end{aligned} \tag{A2}$$

where K is a constant, M is the transition moment per unit electric field amplitude associated with a particular vibrational band, α is the angle the transition moment makes with the c axis, $f = (1/2)(3\langle\cos^2\theta_c\rangle - 1)$, θ_c is the angle the c axis makes with the z axis, and f is the orientational order parameter.

Substituting into eq 1, we obtain

$$R^{ATR} = \frac{E_x^2}{E_y^2} + \frac{E_z^2[f\cos^2\alpha + (1/3)(1-f)]}{E_y^2[(1/2)f\sin^2\alpha + (1/3)(1-f)]} \tag{A3}$$

For thin films (phase 2) on a substrate (phase 1) in air (phase 3), Harrick (1979) has given the equations for the components of the electric field amplitude in thin films where the absorption bands are weak. For the current experiment (angle of incidence of 45°; refractive indices as follows: Ge = 4, lipid film = 1.44, and air = 1.0), these result in relative amplitudes of $E_x = 1.41$, $E_y = 1.46$, and $E_z = 0.728$. The corresponding parametric plot of R^{ATR} vs f for various values of α is shown in Figure A2.

To calculate f from R^{ATR} for a particular band we must know or assume a value for α. If a uniaxial distribution is assumed, f can also be related to a mean angle of disorientation θ by $f = (3\cos^2\theta - 1)/2$. For peptide bond amide I modes, α has been estimated variously at 22° (Nabedryk et al., 1982), 27° (Suzuki, 1971), or 37° (Tsuboi, 1962).

For a model where melittin is assumed to lie within the bilayer as a rigid bent rod, eq A3 is the correct expression for the dichroic ratio for the upper helix. To develop an expression for the dichroic ratio for the lower helix, we consider that the lower helix has fiber orientation around an axis z' which is coincident with the axis of the upper helix. However, the angle of disorientation of the lower helix with respect to z', θ_c, is fixed at 60° because of the 120° bend between the upper and lower helices. Since z' has fiber orientation around z, with an angle of disorientation θ, we obtain

$$\begin{aligned} R^{ATR'} = {} & [E_x^2\{f\sin^2(\alpha/2) + (1-f)/3\}\langle\cos^2\theta\rangle/2 + E_z^2\{f\cos^2\alpha + \\ & (1-f)/3\}\langle\cos^2\theta\rangle]/[E_y^2\{f\sin^2(\alpha/2) + (1-f)/3\}/2] \end{aligned} \tag{A4}$$

REFERENCES

Bello, J., Bello, H. R., & Granados, E. (1982) *Biochemistry 21*, 461–465.

Bernard, E., Faucon, J. F., Dufourcq, J., Duchesneau, L., & Pezolet, M. (1982) *Biophys. J. 37*, 61–62.

Brown, L. R., Braun, W., Kumar, A., & Wuthrich, K. (1982) *Biophys. J. 37*, 319–328.

Cameron, D. G., Casal, H. L., & Mantsch, H. H. (1980) *Biochemistry 19*, 3665–3672.

Dasseux, J.-L., Faucon, J.-F., Lafleur, M., Pezolet, M., & Dufourcq, J. (1984) *Biochim. Biophys. Acta 775*, 37–50.

Dluhy, R. A., Mendelsohn, R., Casal, H. L., & Mantsch, H. H. (1983) *Biochemistry 22*, 1170–1177.

Dufourc, E. J., Smith, I. C. P., & Dufourcq, J. (1986) *Biochemistry 25*, 6448–6455.

Fraser, R. D. B. (1953) *J. Chem. Phys. 21*, 1511–1515.

Fringeli, U. P., & Gunthard, Hs. H. (1981) *Mol. Biol., Biochem. Biophys. 31*, 270–332.

Gremlich, H.-U., Fringeli, U.-P., & Schwyzer, R. (1984) *Biochemistry 23*, 1808–1810.

Harrick, N. J. (1979) *Internal Reflection Spectroscopy*, Harrick Scientific, Ossining, NY.

Hermetter, A., & Lakowicz, J. R. (1986) *J. Biol. Chem. 261*, 8243–8248.

Janiak, M. J., Small, D. M., & Shipley, G. G. (1976) *Biochemistry 15*, 4575–4580.

Kahn, F. J. (1973) *Appl. Phys. Lett. 22*, 386–388.

Lauterwein, J., Brown, L. R., & Wuthrich, K. (1980) *Biochim. Biophys. Acta 622*, 219–230.

Lavialle, F., Adams, R. G., & Levin, I. W. (1982) *Biochemistry 21*, 2305–2312.

Levin, I. W. (1984) in *Advances of Infrared and Raman Spectroscopy* (Clark, R. J. H., & Hester, R. E., Eds.) Vol. II, Wiley-Heyden, London.
Levin, I., Lavialle, F., & Mollay, C. (1982) *Biophys. J. 37*, 339-349.
Mendelsohn, R., & Mantsch, H. H. (1986) in *Progress in Protein-Lipid Interactions*, 2nd ed. (Watts, A., & De Pont, J. J. H. H. M., Eds.) pp 103-146, Elsevier, Amsterdam.
Mendelsohn, R., Dluhy, R., Taraschi, T., Cameron, D. G., & Mantsch, H. H. M. (1981) *Biochemistry 20*, 6699-6706.
Mollay, C., Kreil, G., & Berger, H. (1976) *Biochim. Biophys. Acta 426*, 317-324.
Okamura, E., Umemura, J., & Takenaka, T. (1986) *Biochim. Biophys. Acta 856*, 68-75.
Olson, F. C., Munjal, D., & Malviya, A. N. (1974) *Toxicon 12*, 419-425.
Pincus, M. R., Klausner, R. D., & Scheraga, H. A. (1982) *Proc. Natl. Acad. Sci. U.S.A. 79*, 5107-5111.
Snyder, R. G., Hsu, S. L., & Krimm, S. (1978) *Spectrochim. Acta, Part A 34A*, 395-406.
Terwilliger, T. C., Weissman, L., & Eisenberg, D. (1982) *Biophys. J. 37*, 353-361.
Verma, S. P., Wallach, D. F. H., & Smith, I. C. P. (1974) *Biochim. Biophys. Acta 345*, 129-140.
Vogel, H., & Jahnig, F. (1986) *Biophys. J. 50*, 573-582.
Vogel, H., Jahnig, F., Hoffmann, V., & Stumpel, J. (1983) *Biochim. Biophys. Acta 733*, 201-209.
Weissmann, G., Hirschlorn, R., & Kreakaver, K. (1969) *Biochem. Pharmacol. 18*, 1771-1775.
Yunes, R., Goldhammer, A. R., Garner, W. K., & Cordes, E. H. (1977) *Arch. Biochem. Biophys. 183*, 105-112.

Comparison of cDNA-Derived Protein Sequences of the Human Fibronectin and Vitronectin Receptor α-Subunits and Platelet Glycoprotein IIb†

Laurence A. Fitzgerald,*,‡ Mortimer Poncz,§ Beat Steiner,‡,∥ Stanley C. Rall, Jr.,‡ Joel S. Bennett,⊥ and David R. Phillips‡

Gladstone Foundation Laboratories for Cardiovascular Disease, Cardiovascular Research Institute, Department of Pathology, University of California, San Francisco, California 94140-0608, Division of Hematology, The Children's Hospital of Philadelphia, Philadelphia, Pennsylvania 19104, and The Hospital of the University of Pennsylvania, Department of Medicine, The University of Pennsylvania School of Medicine, Philadelphia, Pennsylvania 19104

Received June 10, 1987; Revised Manuscript Received August 4, 1987

ABSTRACT: The fibronectin receptor (FnR), the vitronectin receptor (VnR), and the platelet membrane glycoprotein (GP) IIb-IIIa complex are members of a family of cell adhesion receptors, which consist of noncovalently associated α- and β-subunits. The present study was designed to compare the cDNA-derived protein sequences of the α-subunits of human FnR, VnR, and platelet GP IIb. cDNA clones for the α-subunit of the FnR (FnR_α) were obtained from a human umbilical vein endothelial (HUVE) cell library by using an oligonucleotide probe designed from a peptide sequence of platelet GP IIb. cDNA clones for platelet GP IIb were isolated from a cDNA expression library of human erythroleukemia cells by using antibodies. cDNA clones of the VnR α-subunit (VnR_α) were obtained from the HUVE cell library by using an oligonucleotide probe from the partial cDNA sequence for the VnR_α. Translation of these sequences showed that the FNR_α, the VnR_α, and GP IIb are composed of disulfide-linked large (858-871 amino acids) and small (137-158 amino acids) chains that are posttranslationally processed from a single mRNA. A single hydrophobic segment located near the carboxyl terminus of each small chain appears to be a transmembrane domain. The large chains appear to be entirely extracellular, and each contains four repeated putative Ca^{2+}-binding domains of about 30 amino acids that have sequence similarities to other Ca^{2+}-binding proteins. The identity among the protein sequences of the three receptor α-subunits ranges from 36.1% to 44.5%, with the Ca^{2+}-binding domains having the greatest homology. These proteins apparently evolved by a process of gene duplication.

Cell adhesion and platelet aggregation are mediated by the binding of adhesive ligands, such as fibronectin and fibrinogen, to a family of cell membrane receptors (Ruoslahti & Pierschbacher, 1986; Hynes, 1987). These adhesion receptors consist of heterodimer complexes of noncovalently linked α-subunits (M_r 140 000-200 000) and β-subunits (M_r 95 000-120 000). Although there are at least 10 receptors in this family, there are only 3 known β-subunits, each of which defines a subfamily of receptors (Hynes, 1987). One subfamily consists of the platelet glycoprotein (GP)[1] IIb-IIIa complex, which is required for platelet aggregation, and the widely

† This research was supported by National Institutes of Health Grants HL 28947 and HL 32254 (to D.R.P.).
* Correspondence should be addressed to this author at the Gladstone Foundation Laboratories, San Francisco, CA 94140-0608.
‡ University of California, San Francisco.
§ The Children's Hospital of Philadelphia.
∥ Present address: Hoffmann-La Roche, Pharmaceutical Research, CH-4002 Basel, Switzerland.
⊥ The University of Pennsylvania School of Medicine.

[1] Abbreviations: GP, glycoprotein; VnR, vitronectin receptor; FnR, fibronectin receptor; FnR_α, fibronectin receptor α-subunit; VLA, very late antigens; SDS, sodium dodecyl sulfate; VnR_α, vitronectin receptor α-subunit; HUVE cell, human umbilical vein endothelial cell; HEL cell, human erythroleukemia cell; SSC, saline-sodium citrate; kDa, kilodalton(s); Tris·HCl, tris(hydroxymethyl)aminomethane hydrochloride.

0006-2960/87/0426-8158$01.50/0